ITU UZMAR AUTONOMOUS BOAT TEAM Technical Design Paper 2022 RobotX Challange

L.Yaman, F.Buyukcolak,E.Begecarslan,B.Ozkuslar, E.Yıldırım,Y.Ibıs,T.Duman,I.Adar, E.Aydemir, R.Emre,O.F.Colak,M.C.Avcu,M.Uygur,D.A.Kocabas

Abstract- **ITU UZMAR Autonomous Boat Team was founded at the Faculty of Naval Architecture and Marine Sciences at 2018.The members our from different engineering departments in order to achieve its goals.Our mission is to carry out works that catch up with the era on unmanned and autonomous vehicle and to represent our country, Istanbul Technical University and the team by achieving permanent success in national and international competitions and our vision is to achieve successful results and to be the winner As the first and only university team to participate in the RobotX Competition.**

I. INTRODUCITON

Our boat,UZMAR BEEAST,has been developed to complete each task in the competition with the most efficient performance. Thanks to the detailed studies on image processing, control, electronic system and mechanical design on the unmanned surface vehicle developed by our team, it has high performance capability. In our article, our team, which has been working on unmanned sea vehicles since 2018, also explains the studies of our team, which has been working in this field, on the unmanned aerial vehicle used in the missions in the competition concept.

II. DEVELOPMENT OF ELECTRICAL HARDWARE

A. Development Criteria of Autonomous Navigaiton System

The hardware for Maritime RobotX Challenge 2022 was designed under the criterias below:

- Design of distributed control systems using calculators with low power consumption.
- Lowering electronics losses by not using inverters.
- Lowering power losses by increased cable radius and shortened cable length.
- Lowering Electromagnetic Interference (EMI) by using twisted pair power cables.
- Aimed to design an advanced motherboard to obtain a system that can work in any condition.
- Localization and choosing ideal types of sensors.
- High capability of lateral movement by basic driving mechanism.

B. Design of distributed control system using calculators with low power consumption

NVIDIA Jetson Xavier used as an on-board image processing computer. Jetson Xavier's power consumption and weight is very low, this contributes power saving and lighter weight on the hull. By harmonizing all hull cameras with Jetson Xavier we achieved high reliability and fast image processing while consuming considerably low power. With the adoption of a distributed control system, we decided to utilize ROS at a much more advanced level with another on-board computer. MSI Cubi-5-10M was chosen for this due to its low power consumption. Also, Cubi-5-10M has much more ports than Jetson Xavier. This contributes to our electronic system design.

C. Lowering electronic power losses by not using inverters

Computers and sensors adopted for control of the hull are 48V, 24V, 19V, 12V, 9V and 5V, only 2 thrusters work with 12V and the other 2 work with 24V. Therefore, there are 6 power systems in the hull. Figure shows the connection of the system. We separated electronic components into three segments for power supplying, autonomous control and motor driving. All these components are placed in waterproof boxes and placed on the hull. By this separated box design we can easily detect and fix failed components. We separated motor electronic components and other electronic components for noise reduction. Other devices like sensors are not supplied directly from the battery but via power electronic cards. We aimed to reduce the length of waterproof wires and make the circuit simpler.

D. Lowering power losses by increased cable radius and shortened cable length

We aimed to build USV to work efficiently although efficiency is not our main concern. For this purpose, we selected 1 or 1,5 bigger AWG sizes. Also, we collaborate with our Mechanical Subteam in ASV cabling work. The Mechanical Subteam modeled the Bee-AST on CAD program then we planned cabling of USV in CAD program.

E. Lowering Electromagnetic Interference (EMI) by using twisted pair power cables

To drive an USV in Autonomous Mode, we need to get clear and uninterrupted data from our sensors. For this reason, we twisted positive and negative cables together to reduce undesired EMI. In addition to that, we reduced the complexity of cabling.

Aimed to design an advanced motherboard to obtain a system that can work in any condition.

We aimed to reduce complexity and increase controllability of our USV. Therefore, we designed a motherboard that can do multiple tasks. Motor driving, temperature control, power conversion, current sensing for Autonomous Drive Mode of our vessel can be done in one card.

In the first version of our USV, we used a driver with class A chopper (a MOSFET to adjust the voltage by switching, and a diode parallel to the load) and two relays for direction adjustment. However, we have changed this usage due to both speed and durability of electromechanical parts. We started using a driver with the H-bridge. Thus, we increased our speed for the change of direction to 25 nanoseconds, which is the switching speed of the MOSFET we use, instead of 10 milliseconds, which is the approximate switching speed of the relays. This has theoretically increased our speed of stopping the engines and turning them in the other direction by 400 times. In addition, both we prevented a possible problem that we may experience due to the limited life of electromechanical parts and increased our driver efficiency.

We also had the opportunity to add an over-current protection system to our new driver. In the first system we set up, we had a system that measures the motor currents and activates the kill switch in case it is high. When this current was too high, it completely blocked our movement and caused our vehicle to work intermittently. Instead, we set up a system that we evaluated on a comparator by measuring the motor current. We connected the comparator output to the microcontroller, which is the controller of our drivers, as an interrupt signal. In case of a current increase, the microcontroller, which receives the cut-off signal, regulates the PWM signal sent to the half-bridge drivers, reducing the current and bringing it to safe levels. Thus, we both protect our system and ensure the continuity of our movement.

F. Development of the Hardware Mechanism

1) Positioning and choosing ideal types of sensors: Visual data is obtained with the OpenCV OAK-D camera placed on the front of the hull. It is aimed to facilitate the depth calculation by placing the camera in the middle of the hull as possible. Thanks to the body suspension, the image remains highly stable. Therefore, the reliability of the obtained data is acceptable.

MICROSTRAIN 3DM GX5-45 model IMU is preferred to receive position, speed, acceleration, direction and temperature information. In this preference, it has been taken in consideration that this model provides raw data output. The IMU is located in the middle of the hull on the symmetry axis of the vehicle so that the acceleration data is not affected while the vehicle is turning. It is planned to add extra GNSS to increase the accuracy of location information.

Aquarin Audio H2C is preferred for underwater listening in Task 2. The hydrophones are attached to the hulls to form an equilateral triangle. By using this figure, it is aimed to reduce the software load.

Velodyne Puck LIDAR VLP-16, which we use for 3D monitoring, has 360º view. The LIDAR is placed high from the payload to prevent blocking 360º view and on the symmetry axis for equal degrees of vision in both directions. Even if the LIDAR is placed high the blindspots will occur. To avoid this situation, it is planned to add a secondary LIDAR.

The placement of the sensors is shown in the Figure 2.

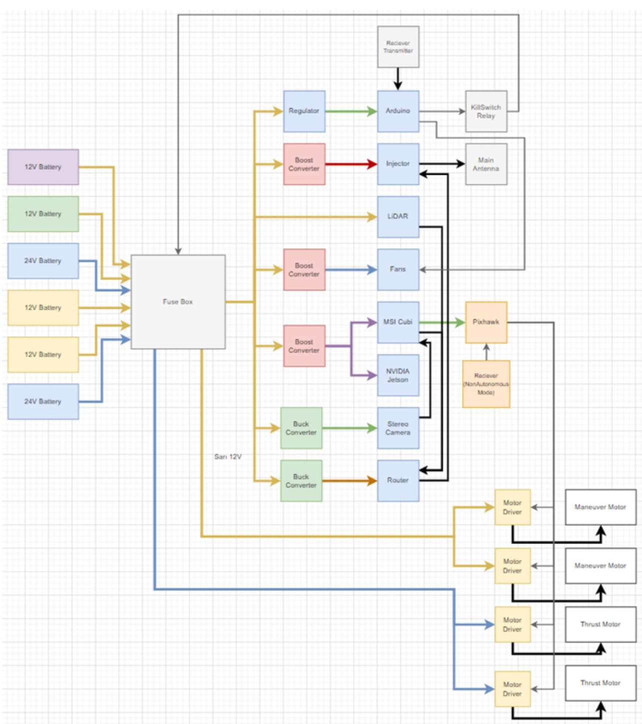

Fig. 1. Electrical Schema

2) Realization of the lateral movement by advanced driving mechanism: In order to increase

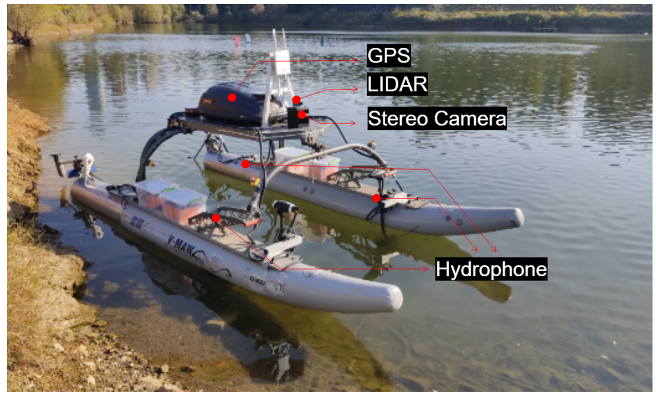

Fig. 2. Placement of Sensors

the capacity of movement and maneuver of the hull, two different propulsion mechanisms with a degree of freedom control in the yaw axis. 2 Haibo D80 electric motors are used to create main propulsion and 2 Haswing Osapian 55 electric motors are used for only maneuvering. We changed the motor rotate speed and torque by predetermined levels with the motor driver.

G. *UAV System Integration*

The UAV that will be used in accordance with the vessel, is capable to do missions completely, in several point of views. We have done improvements for the UAV in mechanical, electrical and software fields to achieve a perfect compatibility with the overall system.

1) Flight Time Estimation: We made flight time calculations by taking the requirements of the missions in account. The requirements include take-off, travel time, area scanning time, the special functions for the missions and landing time.

According to those calculations, we have an estimation of 18 minutes for the flight time. By taking the unexpected events in account, with the 1.5 factor of safety, we need a minimum flight time of 27 minutes.

2) Mechanical Improvement:

a) Extra Battery Compartment: There is an electrical capacity limit to carry LiPo batteries by the plane. Our batteries for the UAV, are in that limit. Since 1 battery in that limit would not be enough for our flight time calculations, we had to add an extra battery to the UAV. After designing the extra battery compartment in 3 dimensions, we printed it by a 3D printer. We placed it on the vehicle and connected the second battery in compatible with the first battery.

b) Gripper Subsystem: Gripper design was an important issue for us because we had to keep our UAV weight within the limit of maximum take-off weight. For this purpose, we made detailed strength and weight analyses. As the result of these analyses, we were able to reduce the weight of the gripper. We made the gripper of elastic TPU material for precisely holding the tin.

3) Hardware Structure:

a) Onboard Computer: There is an onboard flight controller which manages the basic principles of flight on the drone. That controller is not capable of doing hard work such as image processing and mission management. So, we have an onboard computer on the drone to do such work.

Onboard computer has a quad core Arm Cortex-A72 processor and 8GB of RAM on itself. We also use the hardware accelerator for image processing.

b) Stereo Camera Subsystem: We have 5 stereo cameras on the drone. The stereo cameras also have built-in ultrasonic sensors on the board. Every camera module is heading towards a different direction, so the drone is capable of scanning multiple directions at the same time.

c) Telemetry: All the image processing work will be held on the drone directly. So, the telemetry data only includes broadcast information such as current position, compass data and mission messages. We use 433MHz telemetry modules with 18.5dBm transmit power for this purpose.

4) Software Integration:

a) Synchronized Position Control: The drone will get waypoint data during the missions. Alongside, will continue to send position data to the onboard computer. For the purpose of scanning, it will also get the heading information from the onboard computer.

b) Real-Time Attitude Control: For the UAV Replenishment Mission, the drone needs to be controlled dynamically according to the attitude of the drone. So, the onboard computer will get attitude data from the drone at the frequency of 400Hz in the quaternion format. According to the quaternion data, it will control the drone on each axis individually in real-time.

c) Image Processing: All the image processing will be held on the onboard computer. In that way, there will be no need to large bandwidths for transmitting video data over air. The input images for the image processing algorithms will come from the stereo camera subsystem.

d) Mission Management: Mission management is important for overall processes. We have designed an upper system that controls missions in between. So, in case of an occurrence of fail in any mission, the other missions will not be affected. That upper control system is in synchronization with the vessel. Besides, the mission processes themselves are in synchronization with the vessel individually.

e) Take-off and Landing over Vessel: We placed a special lighting system on the drone deck of the vessel for landing precisely and securely in the autonomous mode. Using the stereo camera subsystem, the special lighting will be detected over air. The UAV will be auto-positioned according to the lighting system in real-time. Also, the ultrasonic distance sensors will help the drone for height measurement from the vessel, during the landing process.

f) Scenario of Emergency Case: For an emergency case, we planned a scenario. At the ground station, we are able to get control with the remote controller of the UAV but we have also designed a wireless communication protocol for reporting the situation to the onboard computer. So, the onboard computer will stop autonomous control in emergency.

III. Development of Software

1) Perception: The perception subsystem has four main parts to complete the necessary goals of the coarse elements such as object detection and classification, and color sequence detecting ex, which is the OAK-D Stereo Camera and Velodyne VLP-16 lidar, Hyperspectral Camera and Hydrophone.

Camera Specs	Color camera	Stereo pair
DFOV / HFOV / VFOV	81° / 69° / 55°	82° / 72° / 50°
Resolution	12MP (4032x3040)	1MP (1280x800)
Max Framerate	60 FPS	120 FPS

a) Stereo Camera: BEEAST is equipped with an OAK-D camera for image recognition and localization. The OAK-D stereo camera is capable of simultaneously running advanced neural networks while providing depth from two stereo cameras and color information from a single 4K camera in the center.

b) LIDAR: BEEAST is equipped with Velodyne VLP 16 LIDAR. The LIDAR is mounted on the front of the vehicle. This gives them a clear field of view in front of the vehicle. 9-32 VDC powered the LIDAR and interfaced with the computer via an ethernet connection. The LiDAR has a +15○ to -15○ vertical field of view, with full 360○ horizontal coverage. The system has a range of approximately 100 meters.

c) Hyperspectral Camera: To detect the three different coatings, a HSI camera is used since the difference is just in radiances or reflectances of the surface. NASA's 6SV (pyS6) radiative transfer corrections library is used to convert the radiances to reflectance values. This conversion helps to identify the difference in coatings in any weather since reflectance values have a more distinct graph than radiances.

d) Hydrophones: Locating underwater beacons involves three steps:

1) Picking up and amplifying the audio signal
2) Sampling and processing
3) Calculating the orientation

In order to pick up the sound waves created by the beacon, matching setup of a hydrophone and an amplifier is needed. To sample and process the audio, a dedicated powerful microcontroller is chosen in our case – STM32F446. This microcontroller is capable of sampling 3 channels with the rate of 180khz. After, sampling the audio for small enough time, discrete time Fourier transform is applied on the 3 separate channel data, using ARM CMSIS Math library. DTFT output gives the presence of specified frequency. Considering the time difference between 3 separate hydrophones, as we know the distance and angle between them three, orientation of the frequency source can be inferred.

e) Object Detection and Classification: Object detection and classification have two integrated parts with a lidar and stereo camera. To find buoys and their colors, deep learning is used for object recognition from images. Through various methods, it has been shown by various experiments in both simulation and the real world, that the results from YOLO are far better than other recognition methods in terms of speed and accuracy.

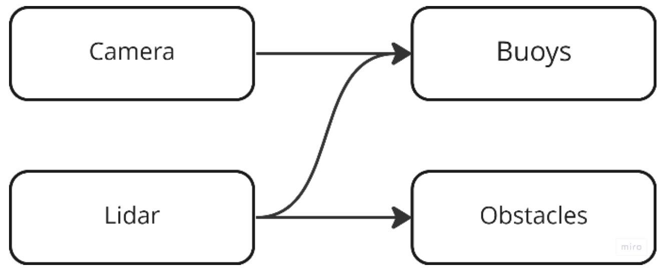

Fig. 3. Placement of Sensors

Camera-based object detection and classification cannot be always enough because of various weather or unidentified obstacles. Therefore, we are also using lidar to detect objects. LIDAR helps them improve the accuracy of object localization. The layout of the object recognition system is shown in Figure.

On the LIDAR side of perception, the raw point cloud data acquired from the VLP16 is inefficient to process because of an excessive number of points and false points from vehicles and the reflection of water. To detect the objects, the pre-processing method should have been used. As part of the pre-processing, we decided to use the Voxel Grid method to decrease the number of points on the cloud and make them organized. Once point cloud data is ready to process, Euclidean clustering is an algorithm that classifies a point cloud into multiple clusters based on Euclidean distance. In our system, PCL's Euclidean Cluster Extraction is performed to detect surrounding objects.

To find a RGB buoy and detect the color sequence, Yolo and OpenCV libraries are used. Firstly, the RGB buoy bounding box is detected by yolo neural network. Once the bounding box of the RGB buoy is detected, a group of pixels with matching colors is searched at the top of the bounding box due to the structure of the RGB buoy. To tune matching color when lighting

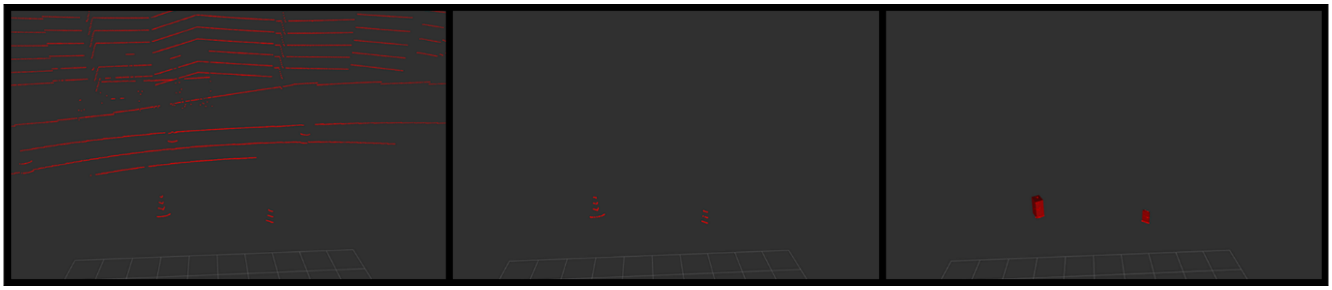

Fig. 4. The point cloud before pretreatment, after pretreatment and the result of Euclidean clustering is shown in the Figure

conditions change, a simple HSV slider that masks the frame by the selected color is used. Then the Color sequence finder starts and tries to verify the sequence.

The detecting dock method has two parts which are finding the dock in a frame and calculating the orientation with the color squares in front of the panel. Since the dimension of the dock and distance of the color squares are known, it's possible to calculate the orientation of the dock in the local frame by just calculating the angle of the line that fits on the location of three color squares in 2-dimensional space. Once the rotation and location of the dock are calculated, we know the location of every part of the dock that includes the corner of entrances.

IV. Control of System

In this section, we represent control system of our vehicle that is call as *BEEAST*. W+e explain general structure of GNC (Guidance, Navigation and Control) system of the our system. We explained State estimation, environment perception in Navigation section, Path generation , local and global path planing in guidance section and control of speed and course, stationkeeping, position control and path following respectively in control section. System structure of vehicle is shown in **figure-5** [5]

A. System Identification

A mathematical model is needed to understand the directional stability and route capability of Wam-v. We are working on 3 degrees of freedom (surge, sway, yaw) to simplify our work in the field of control and navigation. The motion made by the USV in 3 degrees of freedom reveals hydrodynamic force and moment values in addition to the resistance force. Mathematical approaches have been made to determine the parameters in these force and moment equations and to obtain the necessary maneuver derivatives. These approaches were compared with the experimental results and the accuracy value was determined.

B. Guidance

1) Cubic Spline Path Generation: Given waypoints $(x1, y1), (x2, y2)...(xn, yn)$ situated on a 2D map are used to create a path that passes across the waypoints. Formulation for generating cubic spline paths is presented below. Both the first and second derivatives of the route polynomial must be continuous when producing a cubic spline path. These limitations must be considered for interval waypoints.

Each piece-wise polynomial equations can be represent between two waypoints;

$$\begin{aligned}
\theta_1 &= a_{11} + a_{21}x + a_{31}x^2 + a_{41}x^3 \\
\theta_2 &= a_{12} + a_{22}x + a_{32}x^2 + a_{42}x^3 \\
&\vdots \\
\theta_{n-1} &= a_{1(n-1)} + a_{2(n-1)}x + a_{3(n-1)}x^2 + a_{4(n-1)}x^3
\end{aligned} \tag{1}$$

and we consider consider constraints that at start, final and interval points. such as given (x_k, y_k).

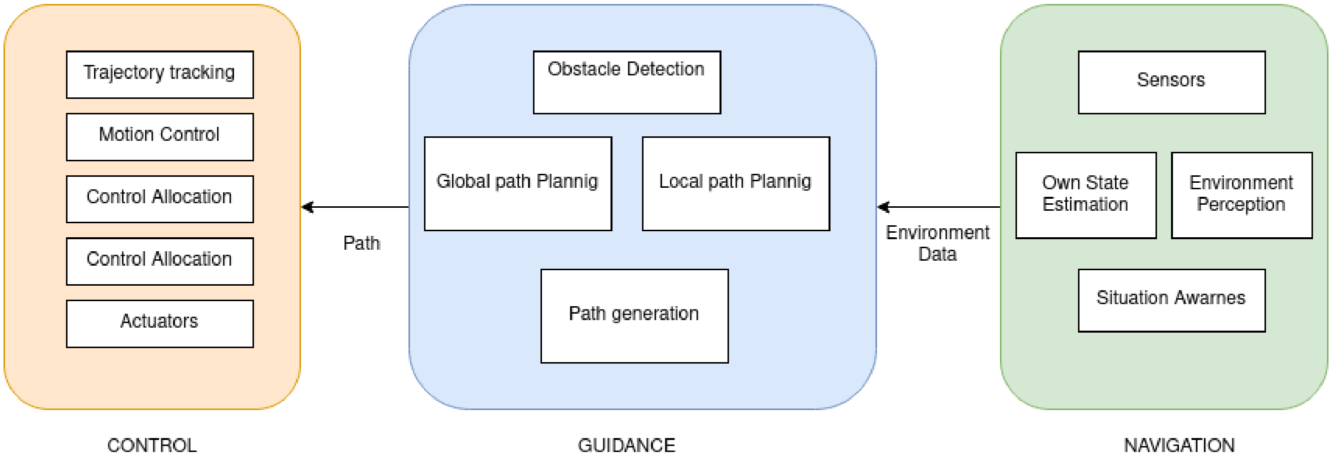

Fig. 5. GNC system of Vehicle

At y_k points, θ_{k-1} and θ_k values have to be equal for polynomial continuity

$$\begin{aligned} a_{4k}x_k^3 + a_{3k_{3k}}x_k^2 + a_{2k}x_k + a_{1k} = y_k \\ a_{4k+1}x_k^3 + a_{3k+1}x_k^2 + a_{2k+1}x_k + a_{1k+1} = y_k \end{aligned} \quad (2)$$

First and second derivatives of equations must be equal

$$\begin{aligned} 3a_{4k}x_k^2 + 2a_{3k}x_k + a_{2k} = 3a_{3k-1}x_k^2 \\ + 2a_{2k-1}x_k + a_{1k-1} \\ 6a_{4k}x_k + 2a_{3k} = 6a_{4k-1}x_k + 2a_{3k-1} \end{aligned} \quad (3)$$

Also, second derivative of polynomial at start and final points equal to zero

$$\begin{aligned} 6a_{41}x_1 + 2a_{31} = 0 \\ 6a_{4n}x_n 2a_{3n} = 0 \end{aligned} \quad (4)$$

C. Navigation

1) Path Following: A path is created with the method described in the guidance section after the points detected by perception according to the task the vehicle is in are translated into global. After the global path is determined, the path is divided into intervals according to the specified δ parameter. δ determined by the length of the vehicle and its maneuverability, that is, the turning radius. The position controller receives waypoints that have been determined at these intervals. Path tracking is provided by the position controller following these waypoints. Using this structure, the global path planner is created.

2) Collision Avoidance: The positions of the objects detected by the lidar and camera sensors mentioned in the Perception section are determined locally. These local points are transformed to global points. Than an obstacle avoidance algorithm is used taking into account the location of these obstacles. We decided to use APF algorithm for USV.

APF Algorithm

The potential field of the force to achieve high-precision path - tracking, and the resultant force (obstacles in the area) of USVs in the force field is written as

$$F_{res} = F_{att} + \sum_i F_{rep,i} \quad (5)$$

where F_{res} is the resultant force, F_{att} is the attractive force of the goal point and $F_{rep,i}$ represents repulsive force from the ith obstacle.

The attractive force provided by the goal point is denoted as

$$F_{att} = \begin{cases} k(p_{goal} - p_{usv}), ||p_{goal} - p_{usv}|| \le \delta \\ \delta k \frac{p_{goal} - p_{usv}}{||p_{goal} - p_{usv}||}, ||p_{goal} - p_{usv}|| > \delta \end{cases} \quad (6)$$

where k is a constant scaling factor, $p_{usv} = [x_{usv} \ y_{usv}]^T$ is the position vector of vehicle $p_{goal} = [x_{goal} \ y_{goal}]^T$ is the choosen desired waypoint position and δ is the threshold value for attractive force.

The repulsive force from the ith obstacle is written as

$$F_{rep,i} = \begin{cases} \nu(\frac{1}{r_i(p_{usv})} - \frac{1}{r_0})\frac{||p_{goal}-p_{usv}||^2}{r_i(p_{usv})}, r_i \le r_0 \\ 0, r_i > r_0 \end{cases} \tag{7}$$

where ν is the coefficient for repulsive force and r_0 refers to obstacle's influence range which determined respect to vehicle length and turn radius. $r_i(p_{usv})$ is the distance from the ith obstacle which vehicle detect.

According to APF algorithm we create our local motion planner to avoidance from detected obstacles.

D. Control

1) Speed and Course Control: Since the vehicle designed for using at low/medium water condition, motion of USV can be reduced motion in x and y axis and and rotation about z axis. So we decided to use linearized 3-DOF motion model. We verified the vehicle's hydrodynamic coefficients, which were retrieved using the system identification method. Coefficient that we extracted by SI method for using in linearized 3-DOF hydrodynamic model. System of model of marine vehicle represent at below [3]

$$M(\dot{\nu}) + D\nu + C\nu = \tau \tag{8}$$

When M represents system mass matrix, D refers damping forces and C shows coriolis forces. M consist of M_{rb} + M_a, C consist of C_{rb} + C_a and D consist of D_l + D_n. Which refers to linear and nonlinear effect matrices shown at the below:

$$M_{rb} = \begin{bmatrix} m & 0 & 0 \\ 0 & m & mx_g \\ m & mx_g & I_z \end{bmatrix} \tag{9}$$

$$M_a = \begin{bmatrix} -Y_{\dot{u}} & 0 & 0 \\ 0 & -Y_{\dot{v}} & -Y_{\dot{r}} \\ 0 & -Y_{\dot{r}} & -N_{\dot{r}} \end{bmatrix} \tag{10}$$

$$C_{rb} = \begin{bmatrix} 0 & 0 & m(x_g r + v) \\ 0 & 0 & mu \\ m(x_g r + v) & -mu & 0 \end{bmatrix} \tag{11}$$

$$C_a = \begin{bmatrix} 0 & 0 & Y_{\dot{v}}v + Y_{\dot{r}}r \\ 0 & 0 & -X_{\dot{u}}u \\ -Y_{\dot{v}}v - Y_{\dot{r}}r & X_{\dot{u}}u & 0 \end{bmatrix} \tag{12}$$

$$D_l = \begin{bmatrix} -X_u & 0 & 0 \\ 0 & -Y_v & -Y_r \\ 0 & -N_v & -N_r \end{bmatrix} \tag{13}$$

$$D_n = \begin{bmatrix} X_{uu} & 0 & 0 \\ 0 & Y_{vv}v + Y_{rv}r & Y_{vr}v + Y_{rr}r \\ 0 & N_{vv}v + N_{rv}r & N_{vr}v + N_{rr}r \end{bmatrix} \tag{14}$$

Vector v includes vehicle states which represents surge velocity (u), sway velocity (v) and yaw rate (r).

$$v = \begin{bmatrix} u \\ v \\ r \end{bmatrix} \tag{15}$$

The origin of body-fixed (vehicle frame) is center of gravity. Vector τ show forces act on the vehicle body. So τ_x refers to produced thrust on the x axis, τ_y is thrust on y axis and τ_z is moment around z axis.

$$\tau = \begin{bmatrix} \tau_x \\ \tau_y \\ \tau_z \end{bmatrix} \tag{16}$$

Proportional Integral Controller PI

For Nonlinear Proportional Integral controller need to first derivative of difference between states

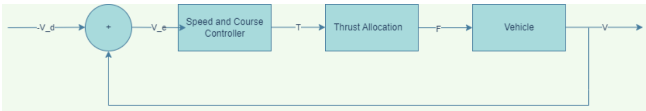

Fig. 6. Control scheme

that in [8] and desired states (input of the controller system) which called error signal. Then integrate the error signal by summing up over time. That will lead to be a saturation so we designed a anti wind-up filter.

$$V_e = V - V_d \tag{17}$$

After obtain the control signal the desired thrust should be allocated. To do this first we calculate the thrust allocation matrix of our system which T as a 3x4 because of using 4 motor. To encounter with this problem, we compute the inverse of matrix by using Pseudo - Inverse method. So we obtain the the forces required for the each one of engines.

$$F = \begin{bmatrix} f_1 \\ f_2 \\ f_3 \\ f_4 \end{bmatrix} \tag{18}$$

2) Position Control: Position control is the method that keeps the vehicle's desired position. system get x,y and ψ value as reference values and controller hold the vehicle on point that is desired. Kinematic eqaution of marine vehicle is used for the position control. $\eta_d = [x_d, y_d, \psi_d]$ is desired pose of the vehicle in the earth-fixed frame, error values can be shown as difference between the desired pose and the vehicle actual pose and controller block output is thust allocation matrix τ.

$$\eta_{error} = \eta - \eta_d \tag{19}$$

Using PD controller, the position error is eliminated

$$\tau = -K_p J(\eta)^T \eta_{error} - K_d[J(\eta)(\eta_{error_k} - \eta_{error_{(k-1)}})] \tag{20}$$

3) Stationkeeping: In order to USV keep its position various factors should be consider :

- Wind forces acting from various directions
- Wave drift forces acting from various directions
- Current drag forces acting from various directions
- Propeller, rudder and thruster efficiency in various directions based on hull interaction, propeller interaction, thruster interaction etc.

Overcome the circumstances we decided to specify a safe diameter in the desired position. Than stationkeeping controller has been developed so that the vehicle does not go out of this safe circle. We determine a position control algorithm for vehicle to make this possible.

V. Mechanical Systems

A. Vehicle Design

Since it is a catamaran type boat, it does not have high maneuverability. However, BEEAST needs to make sudden high maneuvers in the tasks it will perform in the competition. In this context, electronic system development, mechanical and software teams sought the most appropriate solution for this situation. A propulsion system was designed in a way that would not deform the hull and create minimum resistance. Not only the propulsion system, but all the part designs are designed to increase the maneuverability of the vehicle and to minimize the energy loss. In addition, the design, production and positioning of all equipment that will be on the vehicle during the design process were carried out by the mechanic team. In equipment design, it has sought a solution that provides low cost and high strength. In this way, the financial needs of our other teams were benefited in the budget. While the equipment on the vehicle was positioned, the payload was tried to be kept as constant as possible and the vehicle was prevented from heeling and trimming.

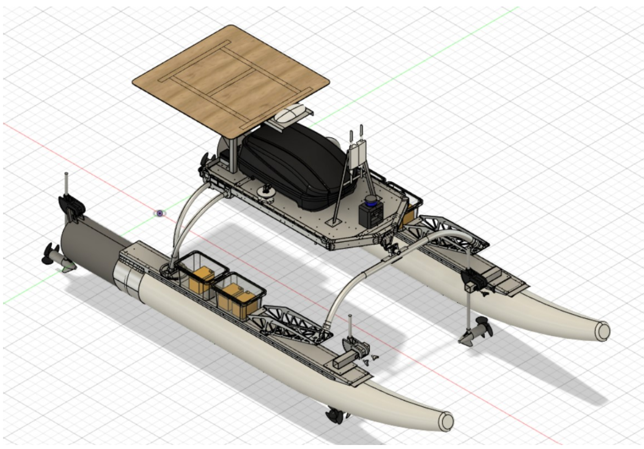

Fig. 7. WAM-V Dimensions

1) Drone Deck: The drone deck is kept in a safe area as far as possible from other equipment so that the UAV can land safely. The stern of the Payload was found to be the most suitable in this area, because it was decided by the team that this is the most fixed point of the payload as a result of the tests. The weight of the UAV is approximately 3.9 kg. A platform that can support this weight is required. Light and high strength aluminum 6061 series was preferred as the material of the platform. This type of aluminum is easily heat-treated thanks to the magnesium silicide it contains. For this reason, there are aluminum series in the form of ”L” profile in the sector. This series of alloys has weldability and relatively good corrosion resistance and moderate strength. A 1.5x1.5 m plywood is considered in the plane where the UAV will land. The stress and displacement values of the Drone Deck under load are calculated using the finite element analysis method below.

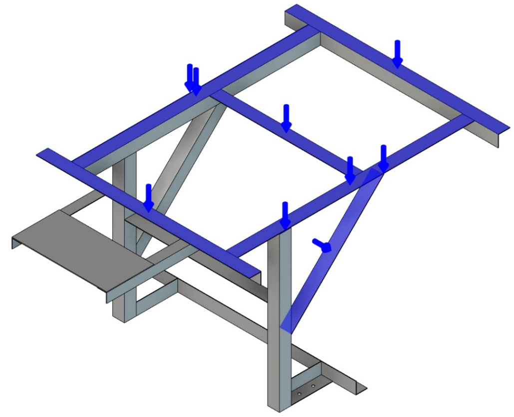

Fig. 8. 40 Newton

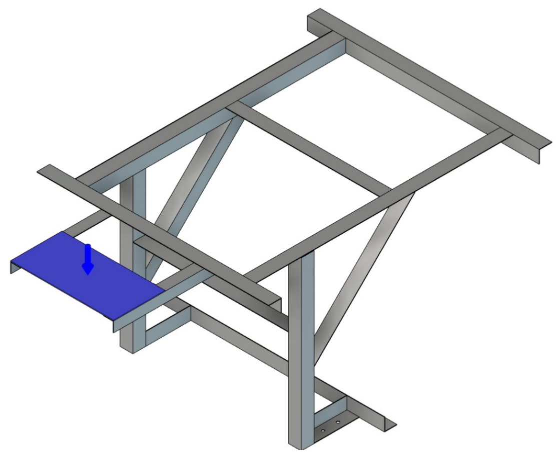

Fig. 9. 10 Newton

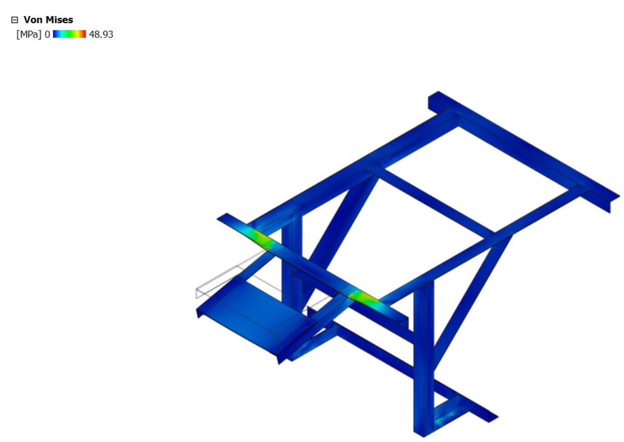

Fig. 10. Von Misses Stress Result

2) Front Engine Holder: In order to increase the maneuverability and course keeping capability of the USV, a 4-engine configuration was pre-

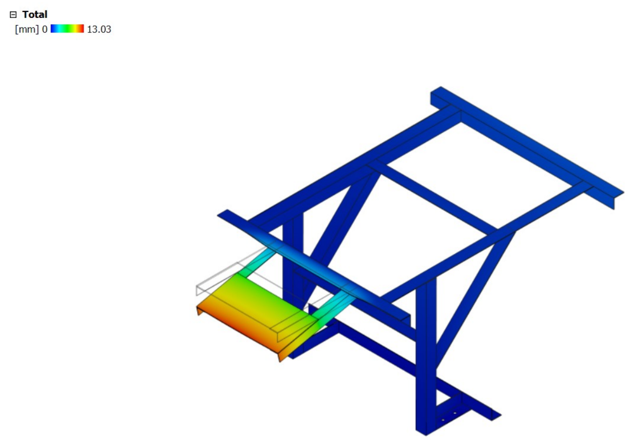

Fig. 11. Displacement Results

ferred. These engines are positioned to propel on the y-axis and are used for maneuvering purposes only. Aluminum 6061 square profiles were preferred in order to place these engines on the vehicle. The stress and displacement values of the front engine holder under load are calculated using the finite element analysis method below.

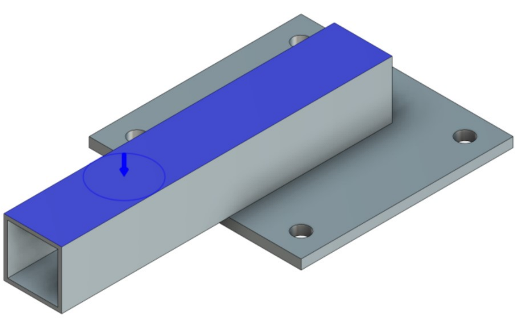

Fig. 12. 150 Newton

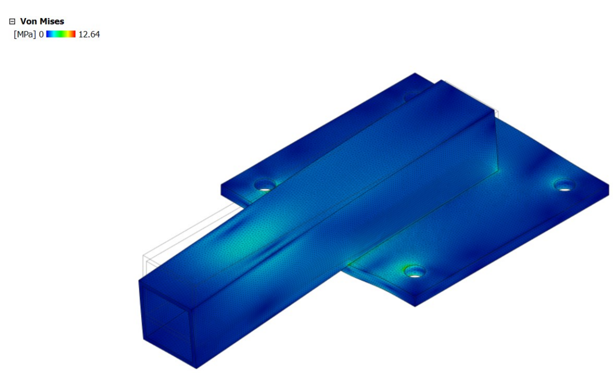

Fig. 13. Von Misses Stress Result

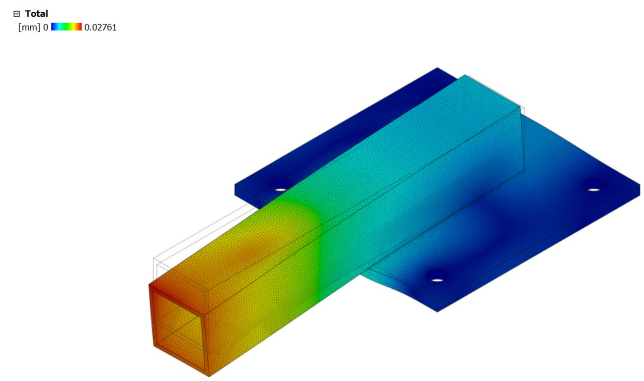

Fig. 14. Displacement Results

3) Wi-Fi Antenna: The stress and displacement values of the wi-fi antenna under load are calculated using the finite element analysis method below.

Fig. 15. 10 Newton

B. Stability

1) Ship Dimensions and Hydrostatic Curves:

a) Ship Dimensions: The following table shows the dimensions of the boat.

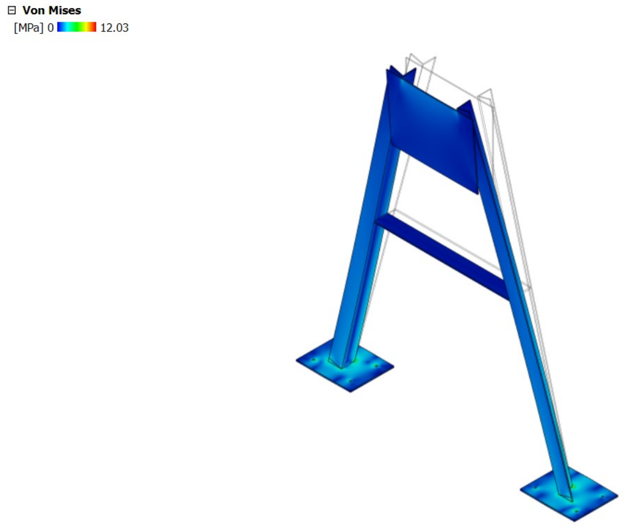

Fig. 16. Von Misses Stress

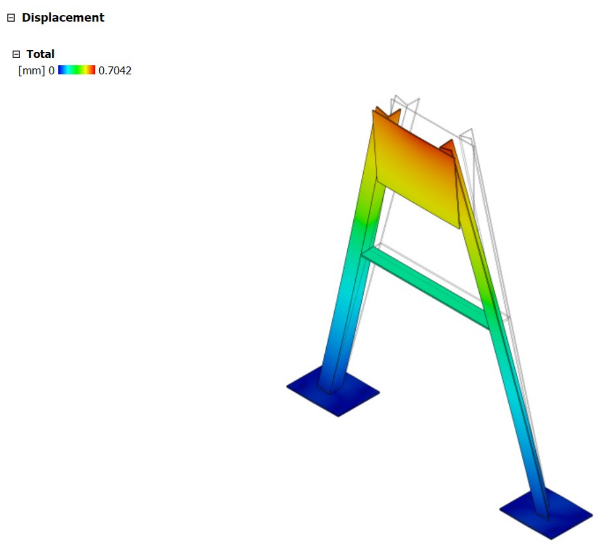

Fig. 17. Displacement Results

ITEM	VALUE	UNITS
LENGTH:	4850	mm
BEAM:	2440	mm
HEIGHT:	127	mm
VESSEL WEIGHT AS NO LOAD	154	kg
NO LOAD DRAFT (ESTIMATED)	8.9	cm
FULL WEIGHT (ESTIMATED)	>268	kg
FULL LOAD DRAUGHT	16.8	cm

Fig. 18. WAM-V Dimensions

b) Hydrostatic Curves: When considering the safety and efficiency of a boat, the characteristics of the boat's form in different loading conditions are very important for both the boat designer and the boat operator. The characteristics of the underwater form of the boat are usually calculated without trim in calm water for all possible waterlines. All of these calculations are called hydrostatic calculations. The results of hydrostatic calculations are also presented in the form of curves using appropriate scales. These curves are called hydrostatic curves.

Section Areas Curves: There are basically two design curves to describe the form and hydrostatic characteristics of a boat: the cross-sectional area curves drawn for each cross-sectional area up to the desired waterline, and the cross-sectional area curves drawn for the design waterline or the loaded waterline. A cross-sectional curve shows the calculated cross-sectional area up to the desired draft (shape of the hull's cross-sectional curves). Then the cross-sectional area is calculated as follows:

$$A_s = 2\int_0^T y(z)dz \sum_{adsa}^{asdasd} asfda \tag{21}$$

Here, y(z) denotes the section half widths. Cross-sectional area curves are used to calculate the untrimmed displacement volume of a ship to the desired waterline. Therefore, the buoyancy distribution throughout the ship is also revealed. In addition, the area under the cross-sectional area curve drawn relative to the design waterline or the loaded waterline also gives the displacement volume of the ship.

Waterlines Curves: The waterline area over which the boat floats can be calculated by integrating the half-widths of the section forming the waterline area across the boat. The waterline area is used to calculate the changes in draft when the ship is loaded. A desired waterline area is calculated from the formula below. [1]

$$Waterline\ ,\ _{WP} = 2\int_d A = 2\int_0^{LWL} y(x)dx \tag{22}$$

A sufficient number of waterlines characterizing all the loading states of the boat must be taken to form the waterline areas curve.

Displacement Curve: The volume below the waterline at which the ship floats is actually a measure of the volume of water displaced by the ship at that waterline. This volume, called the displacement volume, is calculated by numerical integration of the waterline areas to the desired depth.

$$DisplacementVolume,\ \Delta = \int_0^T A_{WP} dz \quad (23)$$

Displacement is calculated by multiplying the density of the water it floats.

$$Displacement,\ \Delta = \rho g \nabla = \gamma \nabla \quad (24)$$

Longitudinal Location of Floating Center Curve: The geometric center of the boat's waterline area is called the swimming centre. The bot trims around this center. The weight average approximation can be used to calculate the longitudinal position of the waterline field center. In that case,

$$LCF = \int x \frac{dA}{A - WP} = 2 \int_0^{L_{WL}} x \frac{y(x)dx}{A_{WP}} \quad (25)$$

Waterplane Area Coefficient Curve: The waterline area slenderness coefficient is obtained by dividing the waterline area by the length and width of the rectangle surrounding this area. If this process is repeated for all water lines, the waterline slenderness coefficient curve will be drawn.

$$C_{WP} = \frac{2 \int_0^{L_{WL}} y(x) dx}{L_{WL} B} \quad (26)$$

Block Coefficient: The block coefficient is a measure of the slenderness of the submerged volume. Therefore, it is defined as the ratio of the volume of the vessel under water to the dimensions of the rectangular prism surrounding this volume.

$$C_B = \frac{\int_0^{L_{WL}} A_s dx}{L_{WL} BT} = \frac{\nabla}{L_{WL} BT} \quad (27)$$

Midship Section Coefficient Curve: The midsection coefficient is a measure of the ship's midsection. Therefore, it is defined as the ratio of the cross-sectional area at any waterline to the dimensions of the rectangle surrounding this area.

$$C_M = \frac{A_s}{BT} \quad (28)$$

Prismatic Coefficient Curve: Since coefficient of a boat alone will not be enough to characterize the hull form, the prismatic coefficient that also shows the forward and stern section is expressed. This coefficient is defined as the ratio of the displacement volume of the ship to the length of the rectangular prism surrounding this volume and the largest central cross-sectional area.

$$C_P = \frac{\nabla}{L_{WL} A_S} = \frac{\nabla}{L_{WL} BT C_M} = \frac{C_B}{C_M} \quad (29)$$

In addition, the vertical prismatic coefficient is a measure showing that the hull form is a 'U' form or a 'V' form. It is defined as the ratio of the ship displacement volume to the depth of the rectangular prism surrounding this volume and the waterline area.

$$C_{VP} = \frac{\nabla}{T A_{WP}} = \frac{\nabla}{L_{WL} BT C_{WP}} = \frac{C_B}{C_{WP}} \quad (30)$$

Vertical Position Curve of Center of Buoyancy: The vertical position of the buoyancy center is one of the important hydrostatic properties as it affects the initial stability of the ship. KB value;
• For each waterline, the total moments of the sections with respect to the base line divided by the displacement volume, or Total moments of the water lines up to the desired water line divided by the displacement volume. It can be calculated as,

$$KB = \frac{\int_0^T x A_{WP}(z) dz}{\nabla} \quad (31)$$

Here, 'z' indicates the height of the waterline relative to the base line.

Longitudinal Position Curve of Center of Buoyancy:

The longitudinal position of the center of buoyancy is usually indicated relative to the center of the boat. It is obtained by dividing the initial moments of the cross-sectional areas by the displacement volume about a given frequency point.

$$LCB = \frac{\int_0^{L_{WL}} xA_s(x)dx}{\nabla} \tag{32}$$

One Centimeter Sinking Tone Curve: An centimeter tonne indicates the weight required for a boat to sink one centimeter parallel. For a ship to sink in parallel, assuming any weight is placed at the buoyancy centre, the displacement will increase and the volume of the sinking portion will be as follows:

$$v = A_{WP} \times t \tag{33}$$

Here 't' denotes the amount of parallel sinking. The additional buoyancy force from the parallel sinking must equal the added weight. In that case,

$$w = \gamma \times v = \gamma \times A_{WP} \times t \tag{34}$$

$$T_{1cm} = \frac{\gamma \times A_{WP}}{100}(\frac{ton}{cm}) \tag{35}$$

In Addition, the change in draught due to parallel sinking is:

$$\delta T_{PB} = \frac{w}{T_{1cm}} \tag{36}$$

One Centimeter Trim Moment Curve: When any weight is loaded, removed, or shifted a certain distance from the boat's buoyancy centre, the resulting moment will cause the ship to rotate around its buoyancy center. This moment is called the one centimeter trim moment.

$$M_{T1CM} = \frac{\Delta \cdot GM_L}{100 \cdot L_{WL}}(ton\frac{m}{cm}) \tag{37}$$

To calculate the trim change that will occur as a result of weight change:

$$\delta Trim = \frac{w \times d}{M_{T1CM}} \tag{38}$$

Here, 'Δ' denotes the displacement of the ship, 'GM_L' the longitudinal metacentric height, 'w' the weight added, subtracted or shifted, and 'd' the offset of the shifted weight or the distance from the center of buoyancy of the added/subtracted weight.

Wetted Surface Area Curve: The wetted surface area of a ship is the area of its surface in contact with the water below the waterline on which it floats. Wetted surface area can be used for ship resistance calculations or for estimating hull weight. To calculate the outer surface area to the desired waterline, the section length from the center to the waterline must be measured in each section, starting at the base line. This section length, called the bow beam length, can be calculated by numerical integration. Therefore,

$$G = \int_0^T \sqrt{1 + (\frac{dz}{dy})^2 dx} \tag{39}$$

Beam length,

$$z = a_0 + a_1 y + a_2 y^2 \tag{40}$$

is defined as a quadratic polynominal:

$$G = \frac{h}{3}(Z_0 + 4Z_1 + Z_2) \tag{41}$$

Here,

$$z_0 = \frac{1}{2h}\sqrt{4h^2 + (n - 4m)^2} \tag{42}$$

$$z_1 = \frac{1}{2h}\sqrt{4h^2 + n^2} \tag{43}$$

$$z_2 = \frac{1}{2h}\sqrt{4h^2 + (3n - 4m)^2} \tag{44}$$

$$and\ m = y_1 - y_2; \quad n = y_1 - y_3 \tag{45}$$

c) Transverse Stability: According to Archimedes' principle, an object that is partially submerged in water exerts an upward force in the vertical direction equal to the weight of the water it displaces. Therefore, in a free-floating body, the weight forces distributed over the body and the buoyancy forces distributed over the wet surface must be in balance. The vector related to the weight of the object is down from the center of gravity and expresses the displacement of the object. The vector related to the buoyancy that will balance this is the vector that acts upwards from the buoyancy center (Figure 1). [4]

The weight distribution of the ship will change when a load on the boat is shifted in any direction, when a load is added/removed anywhere, or a

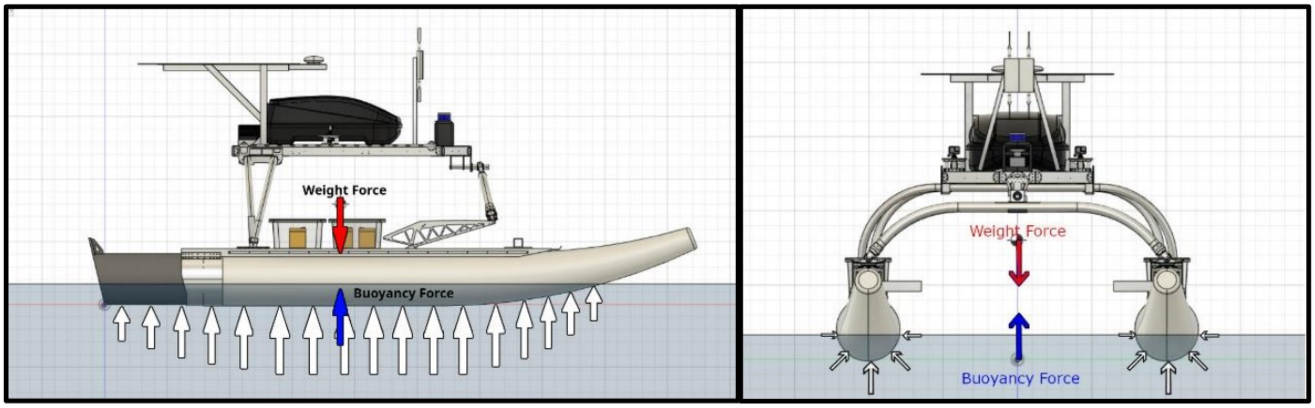

combination of these. When the weight distribution of the ship changes, the position of the center of gravity will also change. When the load is added, the ship's center of gravity will move towards the center of gravity of the load, while when it is removed it will move in the opposite direction to the center of gravity of the load. In the case of weight shifting, it will change parallel to the direction of movement.

This change of the center of gravity will be in the horizontal, vertical and longitudinal directions. The vertical change of the center of gravity can be calculated by averaging the weight. So when considering adding, subtracting or shifting weight, the new position of the center of gravity will generally be according to the formula:

$$KG_1 = \frac{KG_0 \times \Delta_0 + \sum_{i=1}^{n} Kg_i \times (\mp w_i)}{\Delta_0 + \sum_{i=1}^{n} (\mp w_i)} \quad (46)$$

When the center of gravity moves horizontally to port or starboard, the ship will make a certain heel angle in the direction of movement. In this case, the weight force and buoyancy force must be on a straight line for static to be formed. Since the WAM-V autonomous boat is a catamaran, it has very good transverse stability compared to monohull boats. Position of center of gravity in horizontal direction:

$$TCG_1 = \frac{\mp TCG_0 \times \Delta_0 + \sum_{i=1}^{n} Tcg_i \times (\mp w_i)}{\Delta_0 + \sum_{i=1} n(\mp w_i)} \quad (47)$$

d) Longitudinal Stability: At any position along the hull, the fore and aft draft of the ship will change as the weight shifts, adds or subtracts. The ship will trim in the longitudinal direction due to the difference between the fore and aft drafts. The sum of the changes in fore and aft draft also gives the total trim. The hull trims around the waterline area center and this geometric center is called the swim centre. When the ship trims the bow, the bow draft will be greater, and when the stern trims, the stern draft will be greater (Figure 8).

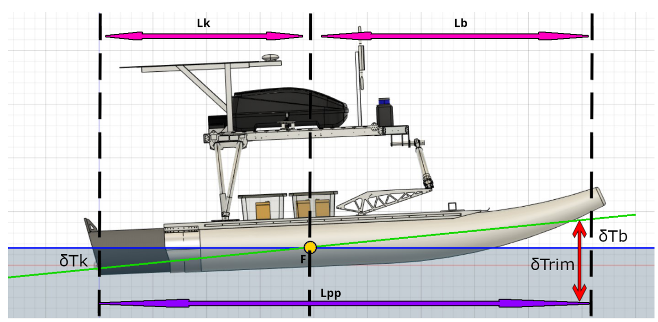

Fig. 19. Trim Diagram

In order to calculate the longitudinal stability of the hull,

• First, a horizontal line is drawn and on this line, the stern, bow, middle of the ship and the swimming center are defined.

• Then, the distances of the stern and bow kaimes from the swimming center are determined.

• The total trim is calculated using the similar triangles that appear.

The following equations are used to find the ship's final draft.

$$T_{b_1} = T = b_0 \mp \delta T_{b_{trim}} \mp \delta T_{b_{pb/c}} \tag{48}$$

$$T_{k_1} = T = k_0 \mp \delta T_{k_{trim}} \mp \delta T_{k_{pb/c}} \tag{49}$$

In the above equations, the first term represents the initial draft, the second term represents the fore and aft draft changes due to trim, and the third term represents the parallel sinking or rising values due to weight. Using the diagram above, the following equations can be written from similar triangles:

$$\frac{\delta T_k}{l_k} = \frac{\delta T_b}{l_b} = \frac{\delta Trim}{L_{pp}} \ here, \ \delta Trim = \frac{w \times d}{M_{T1CM}} \tag{50}$$

If the hull is trimming due to the 'w' weight, the trim moment will be 'w×d'. Therefore, the center of gravity and buoyancy will move to their new positions. Also, the location of the swimming center must be calculated. If the weight addition or subtraction is done at the swimming center, there will be only parallel sinking or rising. In that case,

$$\tan(\theta) = \frac{G_0G_1}{G_0M_L} = \frac{\delta Trim}{L_{pp}} \ here, \ G_0G_1 = \frac{w \times d}{\Delta} \tag{51}$$

The trim change is achived as follows:

$$\delta Trim = \frac{w \times d \ L_pp}{\Delta \times G_0M_L} \ here, \ G_0G_1 = \frac{w \times d}{\Delta} \tag{52}$$

The trim change is achieved as follows:

$$\delta Trim = \frac{w \times d \times L_{pp}}{\Delta \times G_0M_L} = \frac{w \times d}{M_{T1cm}} \ here, \tag{53}$$

$$M_{T1CM} = \frac{\Delta \times G_0M_L}{100 \times L_{pp}} \ ton \cdot m \tag{54}$$

With another approach;

$$\delta Trim = \frac{\Delta \times (LCB - LCG)}{M_{T1CM}} \tag{55}$$

Here, displacement is the displacement after loading or unloading. If the result is negative according to the position of the LCB and LCG values, the LCG value can be found by using the trim up torque value.

$$LCB - LCG = \frac{\delta Trim \times \ M_{T1CM}}{\Delta} \tag{56}$$

$$\Rightarrow LCG = LCB - \frac{\delta Trim \times M_{T1CM}}{\Delta} \tag{57}$$

C. Results

The table below shows the location of the equipment on the vehicle.

Item Name	Unit Mass kg	Long. Arm mm	Trans. Arm mm	Vert. Arm mm
Lightship	154	1971.6	0	481.9
Engine strb. -1-	13.9	0	1015.5	206.4
Engine port -2-	13.9	0	-1015.5	-206.4
Engine strb. -3-	10	3427.4	897.9	447.8
Engine port -4-	10	3427.4	-897.9	-447.8
Batteries strb.	33	1845.6	1005.3	532.7
Batteries port	33	1845.6	-1005.3	532.7
Payload Batt. -1-	6	1146	-252.7	1311.6
Payload Batt. -2-	10	2043	0	1389
Drone Deck	11	1161.1	262.2	1346.8
Wifi Antenna Part	1.9	1128.8	0	2162
Front Engine Holder -1-	2	2511.7	0	1814.6
Front Engine Holder -2-	2	3306.8	922.5	470.2
Lidar Part	1.8	3306.8	-922.5	470.2
GoPro -1-	0.9	2711.3	0	1393.8
GoPro -2-	0.9	1795.3	426.4	1314.7
Portbagage	10	1795.3	-426.4	1314.7
Total Loadcase	310.3	1826.6	0.2	558.2
VCG Fluid				558.2

Fig. 20. The locations of equipments

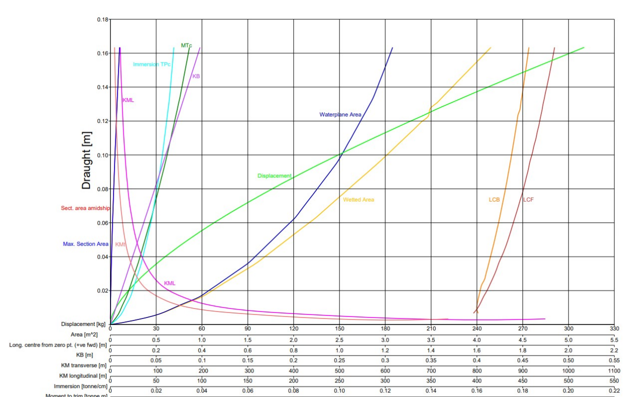

Fig. 24. Positions of KB, KG and KB

RESULTS	VALUES
Draft Amidships mm	163.4
Displacement kg	310.3
Heel deg	0.0
Draft at FP mm	164.6
Draft at AP mm	162.2
Draft at LCF mm	163.2
Trim (+ve by stern) mm	-2.4
WL Length mm	4.041
Beam max extents on WL mm	2430.5
Wetted Area m^2	4.153
Waterpl. Area m^2	3.080
Prismatic coeff. (Cp)	0.850
Block coeff. (Cb)	0.629
Max Sect. area coeff. (Cm)	0.740
Waterpl. area coeff. (Cwp)	0.916
LCB from zero pt. (+ve fwd) mm	1826.8
LCF from zero pt. (+ve fwd) mm	1936.1
KB mm	97.9
KG mm	558.2
BMt mm	9187.9
BML mm	10636.7
GMt mm	8727.6
GML mm	10734.5
KMt mm	9285.8
KML mm	10734.5
Immersion (TPc) tonne/cm	0.028
MTc tonne.m	0.007
RM at 1deg = GMt.Disp.sin(1) kg.m	47265
Max deck inclination deg	0.0284
Trim angle (+ve by stern) deg	-0.0284

Fig. 21. Results

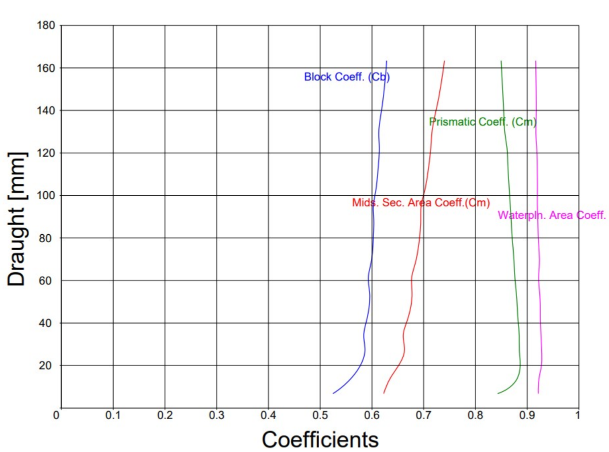

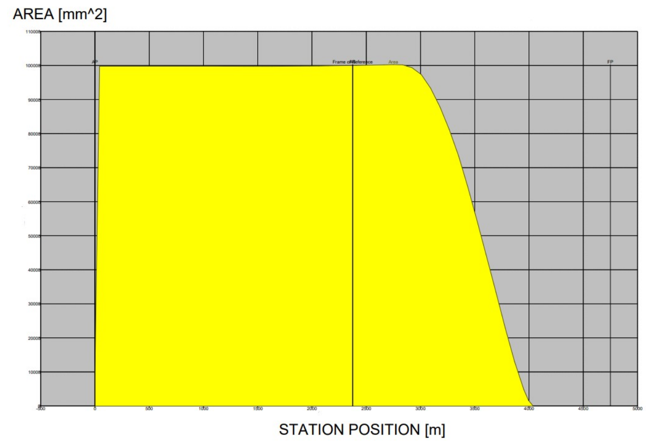

Fig. 22. Section Area Curves

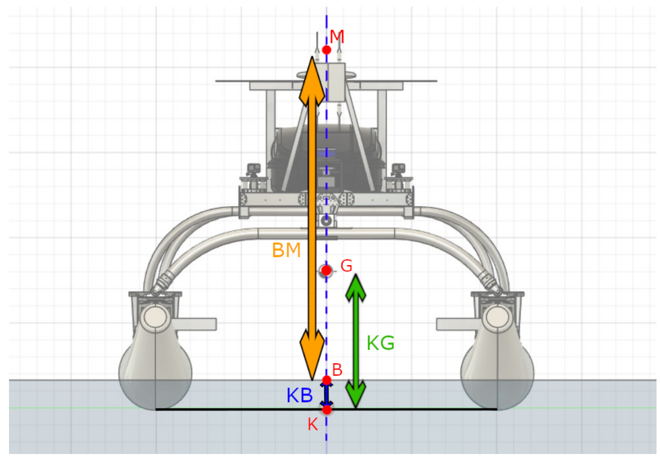

Fig. 23. Positions of KB, KG and KB

D. Resistance

ITTC 1957: This method might be considered a well-known Froude's approach method. In 1957, the ITTC approved the $C_F = 0.075/(logRe - 2)^2)$ frictional boat correlation line, which takes the as the corresponding plank resistance of the boat's wetted surface area. Then it used to determine residuary resistance:

$$C_T = C_F + C_R$$

When the resistance coefficient is dimensionalized, the following result is obtained:

$$C_T = \frac{1}{2} C_T \rho S v^2$$

ITTC 1978: The ITTC Conference in 1978 recommended using the ITTC-1957 frictional formula and combining Hughes' and Prohaska's methods to estimate the form factor. As a result, a boat's overall resistance coefficient without appendages is:

$$C_T = (1+k)C_F + C_R$$

Here, k is the form factor acquired from low-speed measurements using Prohoska's approach, C_F is owing to the ITTC-1957 frictional formula, and C_R is the residual resistance (or particularly wave resistance, C_W) as computed:

$$C_R = C_T - (1+k)C_F$$

Prohaska's Method for Determining Form Factor: Number:

The form factor, k, is defined as follows:

$$k = \frac{C_V - C_F}{C_F}$$

C_F is the corresponding plank frictional resistance in 2D, and C_V is the total viscous resistance coefficient. If no flow separation is present or considered, the total resistance is written as:

$$C_{TM}(Re, Fr) = (1+k)C_{FM}(Re) + C_{WM}(Fr)$$

The wave resistance coefficient in Prohaska's study is considered to be:

$$C_W = sFr^4$$

C_{FM} is used to divide both sides of the resistance equation.

$$\frac{C_{TM}}{C_{FM}} = (1+k) + s\frac{Fr^4}{C_{FM}}$$

As seen in the accompanying diagram, s is proposed as the slope of a straight line. When $\frac{Fr^4}{C_{FM}}$ reaches zero, (1+k) is the value. The resistance calculation of the boat was made using the Maxsurf program. In this program, resistance was calculated using the Slender Body method. Efficiency value was taken as 55 As a result of the results we obtained, the form coefficient of the boat was found to be 1.392

Slender Body: The so-called slender ship or slender body approach is the foundation of this analytical technique. It determines the energy in the vessel's free surface wave pattern and, consequently, the wave resistance of the vessel. Using the ITTC 1957 friction coefficient calculation technique and the chosen form factor, Maxsurf Resistance computes and adds the viscous resistance component to determine the overall resistance. [2]

A slender body, $L << a$, with a usual $2a$ diameter and length L is encircled by a viscous fluid, the motion of which is controlled by Stokes' equations. According to the Stokes paradox, the limit for the infinite aspect ratio $l/a \to \infty$ is unique since there can never be a Stokes flow around an infinite cylinder. [4]

It may be constructed a rough connection between the velocity of the body at each point along its length and the force per unit length that the body is experiencing at that location using the slender-body hypothesis.

Let $X(s,t)$ where s is an arc length coordinate and t is time, characterize the body's axis. Due to the body's slenderness, the force acting on the fluid at its surface may be roughly calculated by a Stokeslet distribution down the axis with a force density of $f(s)$ per unit length. The fluid velocity at the surface next to X(s,t), is considered to fluctuate only over lengths significantly higher than a, and is well-approximated by $\partial X/\partial t$.

The fluid velocity $u(x)$ at a general x point due to such a distribution can be written in terms of an integral of the Oseen tensor (named after Carl Wilhelm Oseen), which acts as a Greens function for a single Stokeslet. Thus,

$$u(x) = \int_0^l \frac{f(s)}{8\pi\nu} \cdot \left(\frac{I}{|x-X|} + \frac{(x-X)(x-X)}{|x-X|^3}\right)ds \tag{58}$$

Asymptotic analysis can then be used to show that the leading-order contribution to the integral for a point x on the surface of the body adjacent to position s comes from the force distribution at

$$|s - s_0| = O(a)$$

Since al, approximating $f(s) \approx f(s_0)$. It is obtained,

$$\frac{\partial X}{\partial t} \sim \frac{ln(\frac{l}{a})}{4\pi\mu} f(S) \cdot (I + X'X') \tag{59}$$

$$where\ X' = \frac{\partial X}{\partial s} \tag{60}$$

The expression can be inverted to give the force density in terms of the motion of body:

$$f(s) \sim \frac{4\pi\mu}{\ln\frac{l}{a}} \frac{\partial X}{\partial t} \cdot (I - \frac{1}{2}X'X') \qquad (61)$$

Two canonical results that follow immediately are for the drag force F on a rigid cylinder (length l, Radius a) moving a velocity u either parallel to its axis or perpendicular to it. The parallel case gives

$$F \sim \frac{2\pi\mu l u}{\ln(l/a)} \qquad (62)$$

while the perpendicular case gives

$$F \sim \frac{4\pi\mu l u}{\ln(l/a)} \qquad (63)$$

with only a factor of two difference.

Note that the dominant length scale in the above expressions is the longer length l; the shorter length has only a weak effect through the logarithm of the aspect ratio. In slender-body theory results, there are $O(1)$ corrections to the logarithm, so even for relatively large values of l/a the error terms will not be that small.

Results

The table below shows the total resistance and effective power values at each speed value.

According to the results obtained, the total effective power required for the boat to travel at 5 knots is 0.997 kW. When reading this value from the table, instead of reading the value opposite the designe speed value, the effective power value at the trial speed was taken by adding +1 knots. Thus, Haibo D80 engines were selected for the aft engines and Haswing Osapian 55 engines were selected for the front maneuvering engines. The Haibo D80 engine has 80 lb of thrust. That is, each has a thrust of 356 N. Haswing Osapian 55 engines also have 55 lb of thrust. That is, it has a thrust of 245 N. Thanks to these values, the desired speed value is reached.

Speed (knot)	Froude Number	Resistance (N)	Effective Power (kW)
0	0	--	--
0.25	0.02	0.21	0
0.5	0.041	0.89	0
0.75	0.061	3.1	0.002
1	0.082	13.29	0.012
1.25	0.102	24.73	0.029
1.5	0.123	34.01	0.048
1.75	0.143	43.76	0.072
2	0.163	51.62	0.097
2.25	0.184	59.09	0.124
2.5	0.204	66.22	0.155
2.75	0.225	66.96	0.172
3	0.245	83.23	0.234
3.25	0.266	78.01	0.237
3.5	0.286	89.92	0.294
3.75	0.307	109.02	0.382
4	0.327	117.44	0.439
4.25	0.347	118.12	0.47
4.5	0.368	118.72	0.5
4.75	0.388	122.92	0.546
5	0.409	131.18	0.614
5.25	0.429	141.8	0.696
5.5	0.45	153.6	0.79
5.75	0.47	165.54	0.89
6	0.49	177.59	0.997

Fig. 26. Results

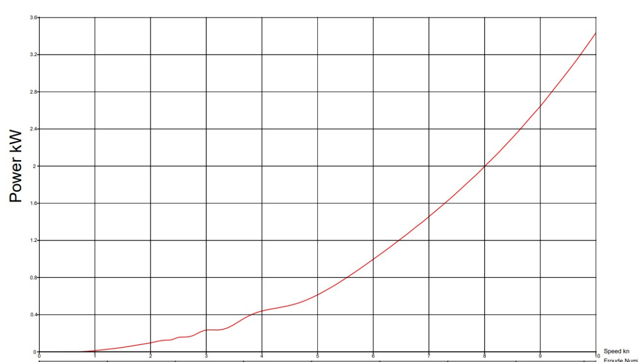

Fig. 27. SpeedFroude No vs Effective Power

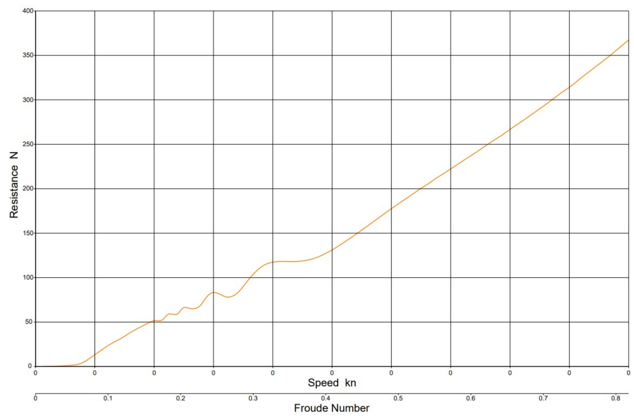

Fig. 28. SpeedFroude No vs Total Resistance

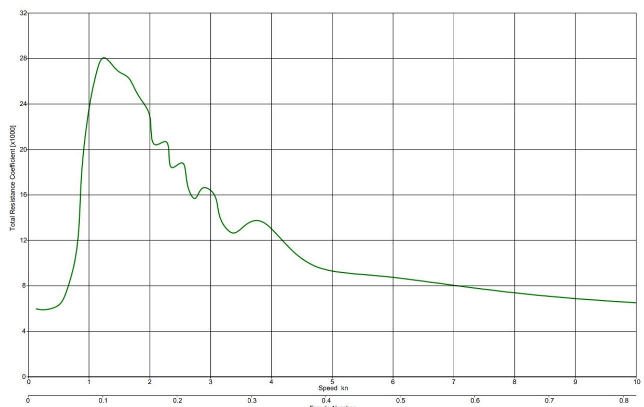

Fig. 29. SpeedFroude No vs Total Resistance Coefficient

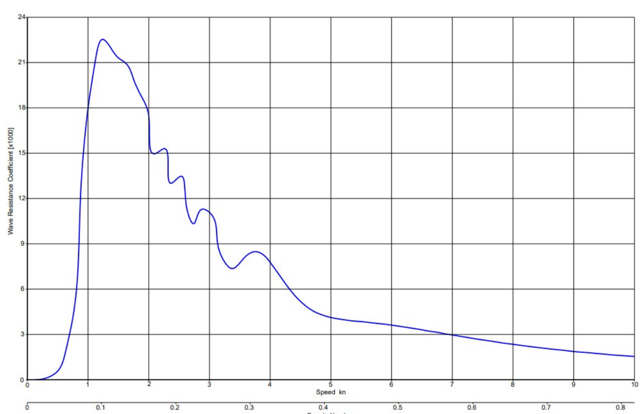

Fig. 30. SpeedFroude No vs Wave Resistance Coefficient

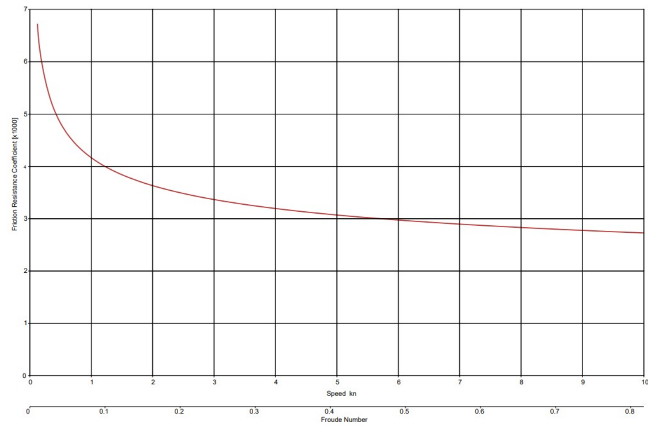

Fig. 31. SpeedFroude No vs Friction Resistance Coefficient

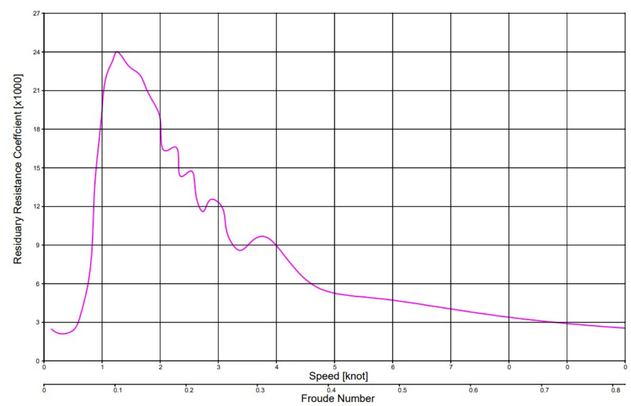

Fig. 32. SpeedFroude No vs Residual Resistance Coefficient

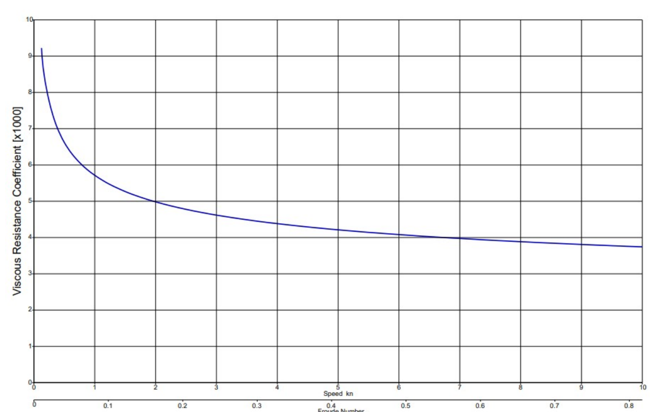

Fig. 33. SpeedFroude No vs Viscous Resistance Coefficient

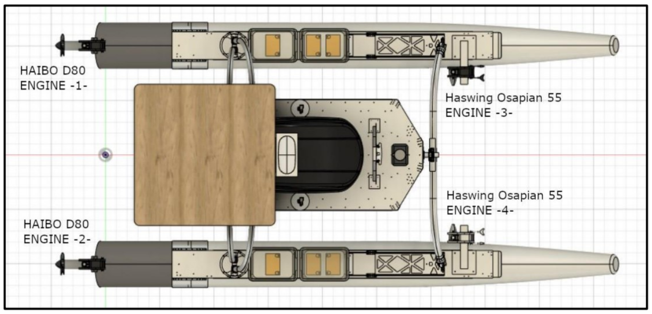

Fig. 34. Engines Locations

References

[1] Hakan Akyıldız. *Gemi ve Deniz Yapıları hidrostatiği ve Stabilitesi Çözümlü Problemler*. ITU Yayınları, 2020.

[2] G. K. Batchelor. "Slender-body theory for particles of arbitrary cross-section in stokes flow". In: *Journal of Fluid Mechanics* 44.3 (1970), pp. 419–440. DOI: 10 . 1017 / s002211207000191x.

[3] Thor I. Fossen. *Handbook of Marine Craft Hydrodynamics and Motion Control*. Wiley, 2011.

[4] Kenneth John Rawson and Eric Charles Tupper. *Basic ship theory*. Butterworth-Heinemann, 2001.

[5] Anete Vagale et al. "Path planning and collision avoidance for autonomous surface vehicles I: a review". In: *Journal of Marine Science and Technology* (2021), pp. 1–15.